Resistance analysis of spherical metal thin films combining van der Pauw and electromechanical nanoindentation methods

Molly Bazilchuk[1,2], Otto Magnus Evenstad[1], Zhiliang Zhang[1], Helge Kristiansen[1,2] and Jianying He[1*]

[1] *Department of Structural Engineering, Norwegian University of Science and Technology (NTNU), Trondheim, 7491, Norway*

[2] *Conpart AS, Skjetten, 2013, Norway*

**Corresponding author: jianying.he@ntnu.no*

Although micron-sized metal-coated polymer particles are an important conductive filler material in anisotropic conductive adhesives, the resistance of the particles in adhesive is not well understood. In this study, a van der Pauw method for spherical thin films is developed and applied to determine the resistivity of 30 µm silver-coated PMMA particles. The resistivity is used to interpret resistance contributions in single particle electromechanical nanoindentation measurements, which simulate the compression particles undergo in application. The resistivity was found to be coating thickness dependent for thin films in the range 60-270 nm. Estimation of the resistance of the metal shell using the measured resistivity did not account for the total resistance measured in electromechanical nanoindentation. We therefore deduce a significant contribution of contact resistance at the interfaces of the particle. The contact resistance is both coating thickness and particle deformation dependent.

Keywords: nanocomposites, resistivity, nanoindentation, conductive adhesives

Introduction

Metal-coated polymer particles (MPS) are a ubiquitous conductive filler component in anisotropic conductive adhesive (ACA) [1]. ACA is used in electronic interconnect where low temperature and fine pitch are required, or when connecting materials that are not wetted by traditional solder, such as transparent conductive oxides [2]. Typical applications include integrated circuit driver mounting in display manufacturing, camera module mounting in mobile phones, and RFID tag manufacturing. During ACA bonding, pressure and heat are

applied, trapping and compressing MPS between opposing bumps and pads. Understanding the relationship between the electrical resistance and mechanical deformation of MPS is essential in minimizing the joint resistance and optimizing ACA properties [3].

In previous works, two methodologies have been used to investigate electrical properties of individual MPS. Electromechanical nanoindentation has been used to measure the electrical resistance of single MPS under compression [4], while four-point probe measurements directly on MPS were used to determine the resistivity of the metal coating [5]. In a continuation of these works, we present an improved method of determining the coating resistivity of MPS, and apply these measurements to further interpret electromechanical nanoindentation data.

Single particle resistance

As illustrated in Fig. 1, the resistance of an MPS under compression can be divided into contact resistance, $R_{contact}$, through the interfaces, and a shell resistance, R_{shell}, through the metal coating [6]. In electromechanical nanoindentation, elements such as the punch and substrate are inevitably encompassed in the four-point measurement and contribute a system resistance R_{system} which is non-negligible for conductive particles. We consider R_{system} to be all resistance contributions external to and not influenced by particle deformation. The measured resistance $R_{measured}$ can thus be expressed as:

$$R_{measured} = R_{shell} + R_{contact} + R_{system} \quad (1)$$

Since both R_{shell} and $R_{contact}$ are dependent on the deformation of MPS, they cannot be decoupled based on the electromechanical nanoindentation measurement alone.

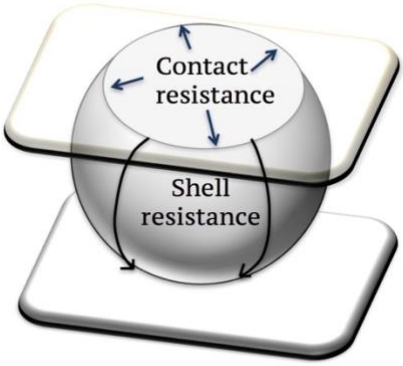

Figure 1: Schematic of the contact resistance and shell resistance through a single MPS under compression.

$R_{contact}$ stems from geometrical constraints of the current (constriction resistance) as well as physical barriers such as oxides at the two interfaces (film resistance).[8] $R_{contact}$ thus depends on the size, morphology and material characteristics of the contact area.[9] In general, $R_{contact}$ will decrease as the deformation (and implicitly the contact area) increases, so $R_{contact}$ is most significant at small deformations.

R_{shell} can be estimated by considering a spherical shell of uniform thickness *t* and radius r_p. Määttanen derived an expression for R_{shell} [10], but the derivation contains contradictory assumptions. At first volume was assumed to be conserved; then the radius of the resulting shape was assumed to be a half- sphere with a radius given by the current deformation. In effect, the volume of the metal shell is continually increased and R_{shell} overestimated. We thus present a self-consistent derivation of R_{shell} as follows. As illustrated in Fig. 2, we assume the spherical shell to be sliced off to a deformation $\frac{\delta}{2}$ on either side, i.e. the volume of the metallic shell decreases with deformation. The resulting shape can be divided in to spherical slices of a thickness $dl = r_p\, d\theta$, where θ is the angle between the slice and the symmetry plane of the sphere. By assuming $t << r$, and applying Ohm's law, we can express the resistance of each slice as:

$$dR = \rho \frac{dl}{A} = \rho \frac{r_p d\theta}{2\pi r t} \tag{2}$$

r is the radius of the sphere at the level of the current slice, given by $r = r_p \cos\theta$. The limits of the spherical shell can be expressed relative to the deformation by $\theta_{max} = \sin^{-1}(1-\varepsilon)$, with the strain given by $\varepsilon = \frac{\delta/2}{r_p}$. By integrating and multiplying by two to include both halves of the sphere, we find:

$$R_{shell} = \frac{\rho}{\pi t}\int_0^{\theta_{max}} \frac{d\theta}{\cos\theta} = \frac{\rho}{\pi t}\ln\sqrt{\frac{2}{\varepsilon}-1} \tag{3}$$

Given that ε can be calculated from electromechanical nanoindentation data, the resistivity-thickness quotient $\frac{\rho}{t}$ (or sheet resistivity) is the main unknown in Eq. 3. Previous analysis assumed ρ equal to that of the bulk metal of the coating. In reality, ρ deviates from the bulk value due to impurities or thickness and grain size constraints in thin metal coatings [11]. Additionally, t may be inhomogeneous within one MPS and varies from particle to particle [5].

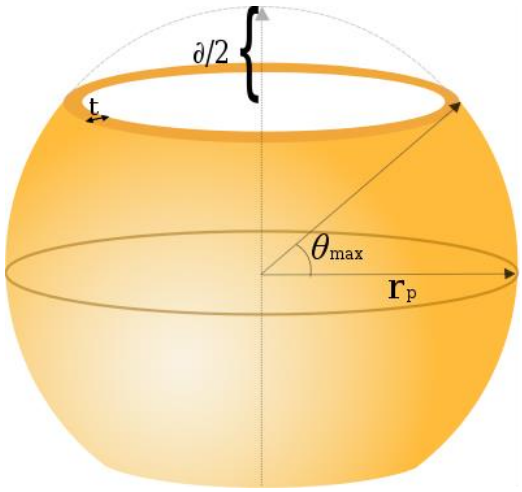

Figure 2: Schematic of the spherical shell model used to calculate R_{shell}.

The first four-point resistivity measurements on individual micron-sized particles were reported by Sun et al. [12]. The probes in their method were fixed, and the particles had to be moved to the probes using a cantilever. Pettersen et al. developed a methodology for performing four-point resistivity measurements using moveable probes attached to micro-actuators in a scanning electron microscope (SEM) [5]. This methodology was successfully applied to MPS. However, the analysis of these four-point measurements was performed using a finite element method, and required an accurate input of probe positions and their contact areas.

The sheet resistivity of flat semiconducting films is commonly measured using the van der Pauw technique, which allows the resistivity of a thin sheet of arbitrary geometry to be determined based on four-point measurements.[13] In this work, Pettersen et al.'s methodology has been extended to implement the van der Pauw technique for measurement of spherical thin metal films.

Experimental

Silver-coated MPS were provided by Conpart AS (Skjetten, Norway). The coatings were deposited using electroless plating. Electromechanical nanoindentation measurements were performed using a Hysitron Triboindenter 950 (Minneapolis, USA) with a custom platinum-iridium flat punch and an electrical contact resistance (ECR) module [4]. 30 µm MPS consisting of a polymethyl methacrylate (PMMA) core with a low cross-linking density of 1% and Ag coatings 60, 100, 150 and 270 nm in nominal thickness were tested.

Greek cross shaped van der Pauw structures were milled using a FEI Helios NanoLab DualBeam focused ion beam (FIB)/ scanning electron microscope (SEM) (Hillsboro, USA). The Greek cross structures had 9×6 µm arms, with a central square of 6×6 µm, as illustrated in Fig. 3. The resistivity measurement was performed across the central square. A preliminary FEM study confirmed that the curved surface did not influence the resistivity calculation for the applicable cross size [7]. The van der Pauw measurements were performed by placing probes on the apexes of the Greek cross using piezoactuated micro robots (miBot BT-11-VP on a miBase BS-43-VP stage, Imina Technologies, Switzerland) which were connected to an Agilent B2909A Precision Source/Measure Unit (Santa Clara, USA). For more experimental details, please refer to the supplementary material Figure S1 and accompanying text.

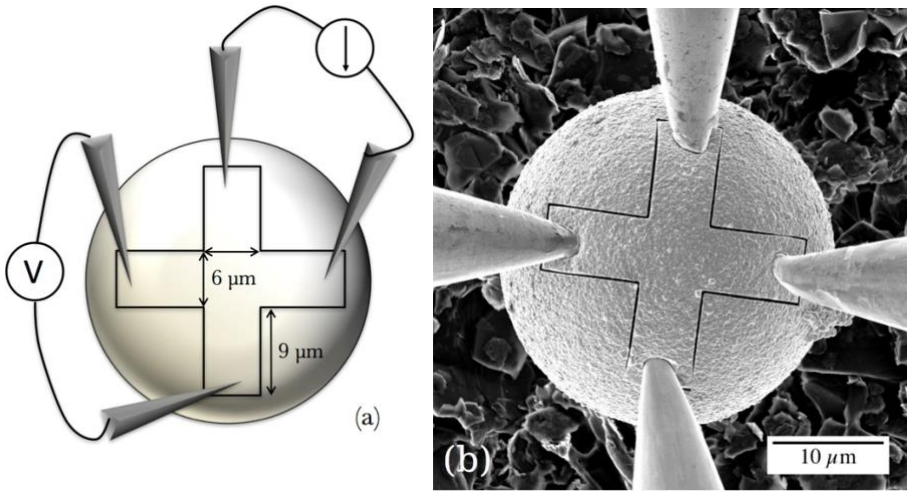

Figure 3: A schematic of the van der Pauw measurement (a) and a micrograph showing a measurement (b).

Results and Discussion

van der Pauw measurements

Fig. 4 summarizes the results of the van der Pauw measurements compared to Pettersen et al.'s measurements on the same MPS [5], as well as resistivity measurements on evaporated Ag thin films [14]. The resistivity values have been normalized relative to the value of bulk silver, 16.2 nΩm [15]. Each van der Pauw data point is the average of 6-8 particles, and the error bars represent the standard deviation. The general trend is that the resistivity decreases with coating thickness. In all cases except one, the van der Pauw results were similar to Pettersen et al.'s measurements within the uncertainty of the measurements. The notable exception is the 100 nm coating, for which Pettersen et al. obtained an inexplicably low resistivity value. The van der Pauw method presented here is less dependent on both probe placement and comprehensive post-processing than Pettersen et al.'s method, which indicates that the original measurements on the 100 nm coating were somehow flawed.

The resistivity of the MPS coatings obtained by van der Pauw method was significantly larger than bulk silver. This could be attributed either to impurities from the plating chemicals, uneven coating thickness causing bottlenecks, or increased scattering due to critical thicknesses comparable to the electron mean free path (EMFP) of silver, 52 nm [11]. Despite averaging over 6-8 particles, the error bars representing the standard deviation in Fig. 3 are large, indicating systematic variations that can be attributed to slight fluctuations from particle to particle in coating thickness and roughness.

The resistivity tends to decrease with coating thickness. The thinner the coating, the more sensitive the resistivity is to local roughness variations that might create current bottlenecks. Furthermore, surface scattering in the thin metal coating could be present [11]. Larson et al. measured the resistivity of Ag thin films epitaxially deposited on mica substrates by evaporation, and fit their results to the Fuchs-Sonderheimer theory for electron scattering in thin films [14]. Interestingly, Larson et al. obtained slightly larger resistivity values for given the film thicknesses. If Fuch-Sonderheim theory applies to our metal coatings, our lower measured values indicate that a larger proportion of electrons are reflected specularly in the MPS coating as compared to the evaporated Ag films. Possibly the silver-polymer interface is more conducive to specular reflection than the silver-mica interface.

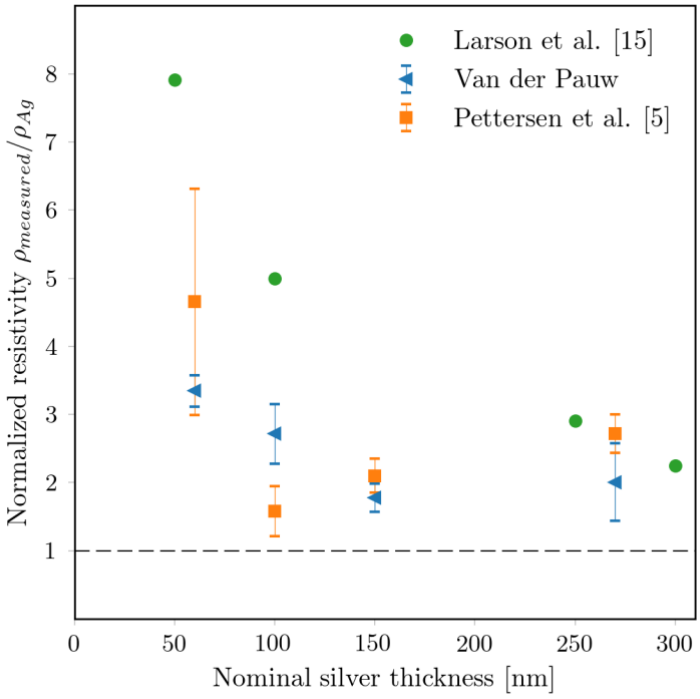

Figure 4: The resistivity of 30 µm MPS with different nominal coating thicknesses measured using the van der Pauw method on Greek cross structure (triangles) and the four-point method (squares). The values are normalized relative to bulk silver.

Comparison to nanoindentation measurements

Fig. 5a shows $R_{measured}$ from electromechanical nanoindentation, with R_{shell} illustrated by the solid areas. R_{shell} was calculated using Eq. 3 in combination with the average resistivity values from the van der Pauw measurements in Fig. 4. The data can be found in the supplementary material, Table S1. The residual resistance

$R_{measured} - R_{shell}$ is consequently the hatched areas. Fig. 5b shows the residual resistance alone, which by Eq. 1 is the sum of the $R_{contact}$ (dependent on strain) and R_{system} (a constant).

The error bars in Fig. 5b are calculated using propagation of uncertainty, combining the standard deviation of the nanoindentation and resistivity measurements. However, the standard deviation of the measured values in this case may be symptomatic of variations in the particle coating rather than error of measurement. The variation in particle coatings is shown in the supplementary material, Figure S2. The initial contact between the particle and probe is only through a few points, and is therefore highly susceptible to small variations in surface roughness. As strain increases, local roughness of the metal in contact area is gradually smoothed out and the resistance is more dependent on the global coating thickness.

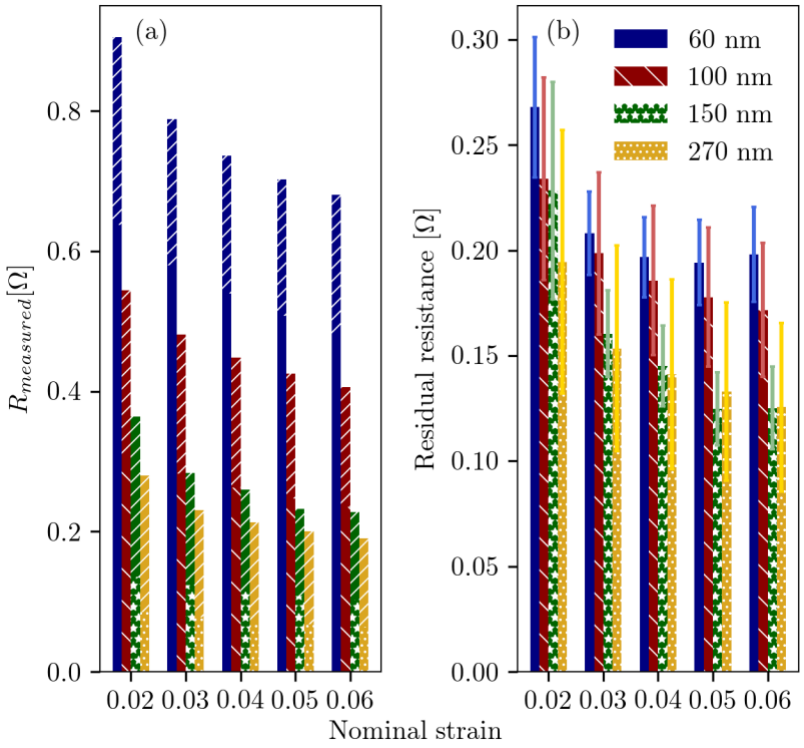

Figure 5: (a) The bars indicate $R_{measured}$ for different coating thicknesses. The solid regions are the calculated R_{shell} value, while the hatched regions are the residual resistance. (b) The absolute value of the residual resistance with error bars indicating the propagation of uncertainty from the nanoindentation and van der Pauw measurements.

The purpose of comparing $R_{measured}$ to R_{shell} is to determine the contribution of the contact resistance. As can be seen in Fig. 5b, the residual resistance decreases as a function of strain, due to increased contact area

and therefore reduced contact resistance. However, the residual resistance remains a non-negligible portion of the $R_{measured}$ for the range of measure strains. At larger strains, the residual is expected to converge to a near-constant value R_{system}, and from Fig. 5b, it is clear that R_{system} can be no greater than 0.15 Ω. It should be noted that the residual resistance is dependent on the R_{shell} model, which contains several simplifications. For the low strains examined in this work, the lateral expansion of the particle and thus the change for the initial spherical shape is negligible [16]. However, this assumption may break down at higher strains, and the Määttänen model may become applicable.

The residual resistance decreases with coating thickness, indicating that the contact resistance is dependent on the coating thickness. Holm showed that the contact resistance is a function of the applied force and surface hardness [8]. A thicker metal shell will increase the hardness in the contact region and thus the force required to reach a given strain, thereby effectively increasing the contact area and hence reducing contact resistance. The spreading resistance, or the additional resistance required for the current to travel from the center to the periphery of the contact area, is larger for thin films [17]. The trend in Fig. 5b can be attributed to a combination of increasing contact area and decreased spreading resistance.

Conclusion

In this study, a method combining electromechanical nanoindentation with the van der Pauw technique has been developed to estimate the resistivity of spherical silver thin films of metal-coated polymer particles. The measured resistivity shows a clear coating thickness dependence, while variability can largely be attributed to variable coating roughness and potentially thickness within one batch. The measured values are generally in agreement with those obtained by the previously developed method. Compared to the previous approach, this method avoids position sensitive and sophisticated finite element calculation based post-processing. The results of the resistivity measurement are used to predict the contribution through the metal shell of the particle under compression. The contact resistance contribution at the interfaces is found to be non-negligible, and is coating thickness dependent.

Acknowledgements

The Research Council of Norway is acknowledged for funding through projects New manufacturing technology for ACF (grant No. 245432) and the support to the Norwegian Micro- and Nano-Fabrication Facility,

NorFab (grant No. 245963). Partial funding has also been obtained from the Programme FP7-NMP-2013-LARGE-7 under grant agreement n°604668 (“Quantiheat”).

References

1. S.-C. Kim and Y.-H. Kim, Curr. Appl. Phys. **13**, S14 (2013).

2. Y. C. Lin and J. Zhong, J. Mater. Sci. **43**, 3072 (2008).

3. Z. L. Zhang, H. Kristiansen, and J. Liu, Comput. Mater. Sci. **39**, 305 (2007).

4. M. S. Bazilchuk, S. R. Pettersen, H. Kristiansen, Z. L. Zhang, and J. Y. He, J. Appl. Phys. **119**, (2016).

5. S. R. Pettersen, A. E. Stokkeland, H. Kristiansen, J. Njagi, K. Redford, D. V. Goia, Z. L. Zhang, and J. Y. He, Appl. Phys. Lett. **109**, (2016).

6. J. H. Constable, in *IPACK03* (2003), pp. 1–8.

7. O. M. Evenstad, Two Novel Methods in the Electrical Characterisation of Single Metal-Coated Polymer Spheres, Norwegian University of Science and Technology, 2017.

8. R. Holm, *Electric Contacts: Theory and Application* (1958).

9. J. H. Constable, IEEE Trans. Components Packag. Technol. **29**, 494 (2006).

10. J. Määttänen, Solder. Surf. Mt. Technol. **15**, 12 (2003).

11. W. Zhang, S. H. Brongersma, O. Richard, B. Brijs, R. Palmans, L. Froyen, and K. Maex, Microelectron. Eng. **76**, 146 (2004).

12. L. Sun, J. Wang, and E. Bonaccurso, Sci. Rep. **3**, 1991 (2013).

13. L. J. van der Pauw, Philips Res. Reports **13**, 1 (1958).

14. D. C. Larson and B. T. Boiko, Appl. Phys. Lett. **5**, 155 (1964).

15. R. A. Matula, J. Phys. Chem. Ref. Data **8**, 1147 (1979).

16. H. Yu, R. Kongsmo, N. Patil, J. Y. He, D. W. Breiby, and Z. L. Zhang, Int. J. Mech. Sci. **128**–**129**, 150 (2017).

17. P. Zhang, Y. Y. Lau, and R. S. Timsit, Proc. 59th IEEE Holm Conf. Electr. Contacts, HOLM 2013 (2013).